PillarNeXt: Improving the 3D detector by introducing Voxel2Pillar feature encoding and extracting multi-scale features

Xusheng Li, Chengliang Wang*, Shumao Wang, Zhuo Zeng, Ji Liu

[a] *Chongqing University, Chongqing, China*
[b] *Chongqing University, Chongqing, China*
[c] *Zhejiang University, Zhejiang, China*
[d] *Chongqing University, Chongqing, China*
[e] *Chongqing University, Chongqing, China*

Abstract

The multi-line LiDAR is widely used in autonomous vehicles, so point cloud-based 3D detectors are essential for autonomous driving. Extracting rich multi-scale features is crucial for point cloud-based 3D detectors in autonomous driving due to significant differences in the size of different types of objects. However, because of the real-time requirements, large-size convolution kernels are rarely used to extract large-scale features in the backbone. Current 3D detectors commonly use feature pyramid networks to obtain large-scale features; however, some objects containing fewer point clouds are further lost during down-sampling, resulting in degraded performance. Since pillar-based schemes require much less computation than voxel-based schemes, they are more suitable for constructing real-time 3D detectors. Hence, we propose the PillarNeXt, a pillar-based scheme. We redesigned the feature encoding, the backbone, and the neck of the 3D detector. We propose the Voxel2Pillar feature encoding, which uses a sparse convolution constructor to construct pillars with richer point cloud features, especially height features. The Voxel2Pillar adds more learnable parameters to the feature encoding,

*Corresponding author
**

Email addresses: lixusheng@cqu.edu.cn (Xusheng Li), wangcl@cqu.edu.cn (Chengliang Wang), maomao123@zju.edu.cn (Shumao Wang), zengz@cqu.edu.cn (Zhuo Zeng), liujiboy@cqu.edu.cn (Ji Liu)

enabling the initial pillars to have higher performance ability. We extract multi-scale and large-scale features in the proposed fully sparse backbone, which does not utilize large-size convolutional kernels; the backbone consists of the proposed multi-scale feature extraction module. The neck consists of the proposed sparse ConvNeXt, whose simple structure significantly improves the performance. We validate the effectiveness of the proposed PillarNeXt on the Waymo Open Dataset, and the object detection accuracy for vehicles, pedestrians, and cyclists is improved. We also verify the effectiveness of each proposed module in detail through ablation studies.

Keywords: point clouds, 3D detector, multi-scale features, pillar feature encoding

---

1. Introduction

Point cloud-based 3D detectors are crucial in autonomous driving [1, 2, 3, 4, 5, 6, 7, 8]. Due to the long detection distance of LiDAR, point clouds are sparse and massive [9]. Current works [10, 11, 12] organize the unstructured point clouds into voxels [13] or pillars [14] and perform feature encoding [10], e.g., Voxel R-CNN [11] and PointPillar [10]. Since the point clouds are sparse, the voxels\pillars only exist at a few locations [15]. So, processing the voxels\pillars by traditional convolution consumes additional computing resources [15], contrary to the real-time requirements of autonomous driving. Current works reduce the computation cost by the sparse convolution [16, 15], which only convolves at the location where the voxels\pillars are present. A frame of point clouds can be organized in voxels\pillars. However, the number of voxels is much larger than that of pillars, and the voxel-based detector needs to utilize the 3D sparse convolution [11, 17], which consumes much more computation than the 2D sparse convolution [11, 17]. The pillar-based detectors that require only the 2D sparse convolution are more compatible with the real-time requirements of autonomous driving [18, 19].

When constructing pillars, first, a simple multilayer perceptron (MLP) is used to expand the features for each point in a pillar [20]; then, the maximum value is taken in each dimension [10, 12]. Compared to the voxel-based feature encoding scheme, the pillar-based feature encoding result has less feature information capacity. It ignores a large amount of point cloud height information, lacking the ability to represent point clouds of different heights [10].

The 3D detection objects such as vehicles, pedestrians, and cyclists vary

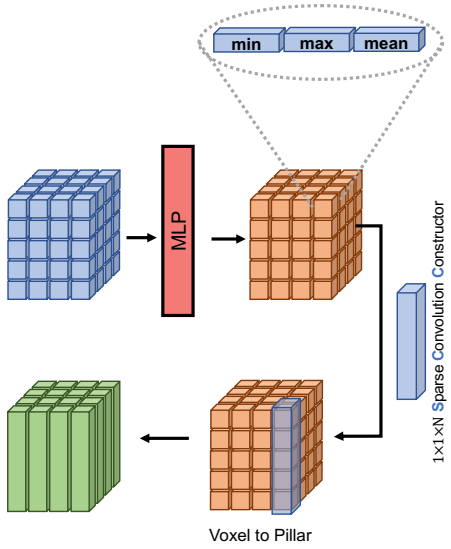

Figure 1: Voexl2Pillar pillar feature encoding. The Voexl2Pillar feature encoding result has the advantages of voxel-based and pillar-based feature encoding, such as the rich information of voxel-based methods and the fewer pillars of pillar-based methods.

significantly in size, and vehicles are oversized [21, 22, 23, 24]. Therefore, extracting large-scale and multi-scale features is essential for accurate 3D object detection [12]. Some image-based object detection [25, 26] and semantic segmentation [27] tasks increase the convolution kernel size to construct large-scale features. However, the computational cost increases rapidly as the size of the convolution kernel enlarges [25, 27, 23]. Due to the real-time requirements, the large-size convolution kernel is seldom used in the backbone of the 3D object detection [12]. However, constructing large-scale features is necessary to accurately detect large-size objects, such as vehicles. [28].

The pillar-based detectors usually extract multi-scale features by performing step-by-step down-sampling in the backbone [12]. The layer at the tail of the backbone has a large receptive field, which can construct long-range features for large-size objects [10, 12]. For example, VoxelNeXt [12] utilizes six layers of step-by-step down-sampling in the backbone, and the last layer obtains a large receptive field to construct long-range features for large-size objects. Moreover, the features output from the last three layers are combined to obtain multi-scale features, which improves the detection accuracy of multi-scale objects. However, some objects with fewer points are further lost during the down-sampling, resulting in an inability to adequately

construct large-scale features of these objects at the tail of the backbone. Therefore, the construction of multi-scale features should be performed at the early layer of the backbone.

We propose the PillarNeXt to extract multi-scale and large-scale features at each layer of the fully sparse backbone. The feature encoding, the backbone, and the neck are redesigned. First, we propose the Voxel2Pillar feature encoding method, which combines the advantages of voxel-based and pillar-based feature encoding methods. It uses the proposed sparse convolution constructor to construct pillars from voxels with richer features. Second, in designing the fully sparse backbone, we avoid expanding the receptive field by increasing the size of the convolutional kernel, thus ensuring real-time 3D object detection. The backbone adopts the step-by-step down-sampling; each layer uses the proposed multi-scale feature extraction module. Each multi-scale feature extraction module contains a dense large-scale feature extraction block and several large-scale feature extraction blocks to achieve fine-grained and coarse-grained large-scale feature extraction, respectively. The backbone has achieved the extraction of multi-scale features throughout the entire process, improving the accuracy of object detection while ensuring real-time performance. Finally, we propose the sparse ConvNeXt to extract multi-scale features in the neck. With a slight modification, significant performance improvements are obtained.

Our contributions are summarized as follows:

1. We propose the PillarNeXt, which redesigns the feature coding, the backbone, and the neck. The network significantly improves the accuracy of the 3D object detection.

2. We propose the Voxel2Pillar feature encoding, which combines the advantages of the voxel-based and the pillar-based feature encoding. The proposed sparse convolution constructor constructs pillars from voxels that contain richer features.

3. A fully sparse backbone is proposed to extract multi-scale and large-scale features at each layer.

4. We use the proposed sparse ConvNeXt to extract multi-scale features in the neck, and the slight modification significantly improves the performance.

2. Related work

In this section, we first review recent 3D detectors and pillar-based detectors. Then, we review sparse convolution and multi-scale feature extraction methods.

2.1. 3D detectors

PV-RCNN [17] deeply combines a 3D voxel convolutional neural network with PointNet-based set abstraction to learn more discriminative point cloud features. It exploits the efficient learning and high-quality proposals of the 3D Voxel CNN and the flexible receptive field of the PointNet-based network. In contrast to traditional pooling operations, RoI-grid feature points encode richer contextual information to estimate object confidence and location accurately. Voxel R-CNN [11] proposes that coarse-grained voxels can provide sufficient detection accuracy. A simple but effective voxel-based framework is designed using voxel features in a two-stage method. The proposed method substantially increases the speed of object detection while maintaining accuracy. CenterPoint [29] uses points to represent, detect, and track 3D objects. It uses a keypoint detector to detect the object's center, which is regressed to additional properties, including 3D size, 3D orientation, and velocity. In the second stage, it uses additional point features on the object to improve these estimates. CenterPoint improves previous state-of-the-art techniques by 10-20% when running at 13 Frames Per Second (FPS). Part A^2 [30] is a 3D detector for point clouds. It uses the intra-object part information to learn distinctive 3D features and improves the performance of 3D object detection via RoI-aware pooling and sparse convolution.

2.2. Pillar-based 3D detectors

Real-time and high-performance 3D object detection is crucial for autonomous driving. The pillar-based detectors consume less computational resources by using only 2D convolution. PointPillar [10] is a widely deployed detector for 3D object detection that balances speed and accuracy. The pillars are converted to pseudo-images, and feature extraction is performed using a 2D detection network. The PointPillar's detection speed reaches 62Hz. PillarNet [31] is a real-time and high-performance pillar-based detector using only 2D convolution. The proposed pillar network consists of an encoding network for pillar feature learning, a neck network for spatial semantic feature fusion, and the usual detection head. The detection performance is

improved thanks to the designed orientation-decoupled IoU regression loss and IoU-aware prediction branch. Sparse voxel features need to be densified and processed by a dense prediction head, requiring additional computational costs. VoxelNext [12] performs fully sparse 3D object detection, predicting objects directly based on sparse voxel features without sparse-to-dense conversion or NMS post-processing. The detector balances speed and accuracy, demonstrating that the fully sparse voxel-based representation works well for 3D object detection and tracking. A pillar-based version of the VoxelNext is also provided, and the speed and accuracy achieved are competitive.

2.3. Sparse Convolution

Sparse convolution is widely used in point cloud tasks because it saves a lot of computational costs by performing convolution computations only at non-empty locations [32, 33, 34]. Sparse convolution consists of spatially sparse convolution [15] and submanifold sparse convolution [16]. Spatially sparse convolution [15] reduces the computation by considering only the positions of non-empty elements in the data. The convolution kernel's receptive field is restricted to the data's non-null elements, and the convolution operation is performed only at these locations. Spatially sparse convolution [15] makes the convolution operation more efficient and suitable for processing sparse data. However, the use of spatially sparse convolutions leads to an increase in the sparsity of the data. Submanifold sparse convolution [16] also focuses only on the non-null elements in the data and convolves only when a non-null element appears in the center of the convolution kernel and thus does not lead to an increase in sparsity in the convolution results.

2.4. Multi-scale features

Multi-scale feature extraction is essential in image-based object detection tasks. However, due to the task's real-time requirements, large-size convolutional kernels are generally not used in the backbone. Feature pyramid networks [35] are frequently used in image-based detectors to extract object features of different sizes. Numerous recent works [36, 37, 38] have used feature pyramid networks and their variants to address the problem of small and multi-scale objects in object detection. DeepLab [39] introduces dilated convolutions in image-based semantic segmentation, effectively expanding the receptive field to obtain more context information without increasing the parameters and computation cost. Payal Mittal et al. [40] used dilated convolutions to study contextual information of specific small-sized objects.

The complex detection problem caused by large differences in object scales, small sizes, and occlusions is solved. TridentNet [41] investigates the effect of the receptive field on scale variation in object detection and constructs a multi-branch structure. Each branch uses dilated convolutions with different scales to improve object detection accuracy.

3. PillarNeXt

In point cloud-based 3D object detection tasks, extracting multi-scale features is essential because vehicles, pedestrians, and cyclists vary significantly in size [23]. Existing 3D detectors typically use feature pyramid networks to construct large-scale features at the tail of the backbone [12]. However, some long-range objects, including fewer point clouds, will become more sparse in the backbone. We aim to construct a pillar-based 3D object detector. The PillarNeXt extracts multi-scale features at each layer in the backbone to construct a fast and efficient 3D detector. We have also redesigned the feature encoding and the neck of the PillarNeXt.

This section proposes the PillarNeXt. Sec.3.1, Sec.3.2.1, and Sec.3.2.2 present the Voxel2Pillar feature encoding, the fully sparse backbone, and the neck, respectively. Finally, the structure of the PillarNeXt is presented in Sec.3.4.

3.1. Voxel2Pillar feature encoding

Voxel-based and pillar-based feature encoding methods divide the raw point clouds in the grids and then encode the points in each grid [13, 14, 10]. Voxel-based feature encoding divides the raw point clouds according to the horizontal and vertical dimensions and requires the 3D convolution for the voxel feature extraction [15, 16]. Pillar-based feature encoding methods only divide the raw point clouds according to the horizontal dimension and only require the 2D convolutions for the pillar feature extraction [10]. The number of pillars is considerably smaller than the number of voxels. The 2D convolution kernel with fewer parameters is computationally faster than the 3D convolution [10]. Therefore, pillar-based feature encoding methods [14] are more favorable for constructing high-speed 3D detectors.

Pillar-based feature encoding methods [10, 42, 43] divide the raw point clouds into grids according to the pillar size. Then, the points in each grid are encoded. It can be formulated as:

$$Pm_{(i,j)} = ReLU(BatchNorm(MLP(Pi_{(i,j)}))) \tag{1}$$

$$Feature_{(i,j)} = max(Pm_{(i,j)}) \tag{2}$$

In Equation 1, $Pi_{(i,j)}$ represents point clouds in a grid, i and j represent the coordinates of the grid. $MLP()$ is a simple MLP that expands the features of each point in the grid. $BatchNorm()$ and $ReLU()$ is the Batch Norm and the ReLU activation function. $Pm_{(i,j)}$ is the feature extension result. Equation 2 represents obtained the maximum values of each dimension of $Pm_{(i,j)}$. $Feature_{(i,j)}$ is the feature encoding result called pillar.

Our proposed feature encoding method can be formulated as:

$$Feature_{(i,j)} = [max(Pm_{(i,j)}), min(Pm_{(i,j)}), mean(Pm_{(i,j)})] \tag{3}$$

Equation 3 represents obtaining the maximum, the minimum, and the average values of each dimension of the feature extension result $Pm_{(i,j)}$ and concatenating them to obtain the enriched feature encoding result $Feature_{(i,j)}$. The proposed method encodes raw point clouds in pillars with richer features than the widely used Pointpillar's feature encoding block [12, 31, 10].

However, pillar-based feature encoding has apparent drawbacks compared to voxel-based methods, such as coarse feature granularity and lack of expressiveness in vertical dimensions [10, 12]. Therefore, we propose the Voxel2Pillar feature encoding. The approach combines the advantages of both encoding methods, resulting in encoded pillars that contain richer features and are more expressive in the vertical dimension.

The proposed Voxel2Pillar feature encoding is shown in Fig. 1. It is formulated as:

$$Vm_{(i,j,k)} = ReLU(BatchNorm(MLP(Vi_{(i,j,k)}))) \tag{4}$$

$$Vf_{(i,j,k)} = [max(Vm_{(i,j,k)}), min(Vm_{(i,j,k)}), mean(Vm_{(i,j,k)})] \tag{5}$$

$$Pillar_{(i,j)} = ReLU(BatchNorm(Spconv_{(N,1,1)}(Vf_{(i,j,:)}))) \tag{6}$$

Firstly, the raw point clouds are divided into three-dimensional grids. $Vi_{(i,j,k)}$ represents point clouds in a three-dimensional grid, i, j, and k represent the coordinates of the three-dimensional grid. Then, a simple MLP is used to expand the features of points in each three-dimensional grid. Equation 5 represents obtaining the maximum, the minimum, and the mean values of each dimension of the feature extension result $Vm_{(i,j,k)}$ and concatenating

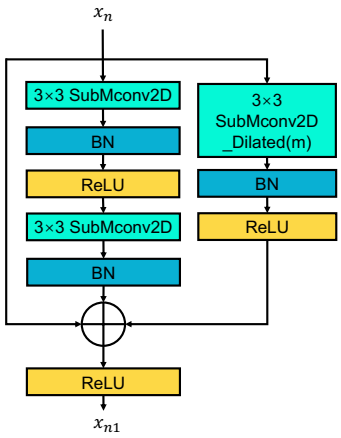

Figure 2: The large-scale feature extraction residual block (LSFE-Res-Block). LSFE-Res-Block consists of the residual branch, dense feature extraction branch, and large-scale feature extraction branch. SubMconv2D denotes the submanifold sparse convolution. SubMconv2D_Dilated denotes the dilated submanifold sparse convolution, and m denotes the dilation coefficient.

them to obtain the new feature vector $Vf_{(i,j,k)}$. Equation 6 represents the proposed sparse convolution constructor. It consists of a $1 \times 1 \times N$ spatially sparse convolution, a Batch Norm, and a ReLU activation function; N is the maximum number of voxels in the vertical dimension. The sparse convolution constructor merges the voxels in the vertical dimension to obtain the pillar $Pillar_{(i,j)}$. Since the point clouds are sparse, not many computations are performed despite the large size of the convolution kernel.

3.2. Backbone

3.2.1. Large-scale feature extraction residual block

Extracting multi-scale and large-scale features of objects at the early backbone layer is conducive to improving the detection accuracy of objects of different sizes [12]. Large-scale features of the object are usually constructed by expanding the receptive field [40]. However, enlarging the convolution kernel size increases the number of parameters and brings significant computational costs, contrary to the real-time requirement of the autonomous driving task [39, 40].

The dilated convolution [44] expands the coverage of the convolution kernel by inserting spaces between the kernel elements and obtains a large re-

ceptive field without additional computational cost. Therefore, inducting dilation convolution in the feature extraction block effectively expands the receptive field to learn large-scale object features without significantly increasing computational effort.

The proposed large-scale feature extraction residual block (LSFE-Res-Block) is shown in Fig. 2. It consists of three branches: the main feature extraction branch, the residual branch, and the large-scale feature extraction branch. The main feature extraction branch consists of two 3×3 submanifold sparse convolutions [16] to extract the fine-grained features of pillars. The residual branch is utilized to prevent network performance degradation [45]. In particular, instead of adding the dilation convolution directly on the main branch, a separate branch with dilation convolution is utilized to extract large-scale features because the dilated convolution probably causes local information loss, and the acquired over-range features may be uncorrelated. Therefore, the main branch extracts the fine-grained features, and the large-scale feature extraction branch helps establish long-range feature relationships for large-size objects. As shown in Fig. 2, the large-scale feature extraction branch utilizes a 3×3 submanifold sparse dilation convolution [16], where m denotes the dilation rate. The dilation rate gradually increases to incrementally enlarge the receptive field and realize the multi-scale features construction. Submanifold sparse convolution [16] focuses on non-null elements in the data and convolves when a non-null element appears in the center of the convolution kernel. The block utilizes the submanifold sparse convolution, which does not lead to an increase in the sparsity of the convolution result at each branch. Eventually, all branch outputs are aggregated to construct features with fine-grained features and coarse-grained large-scale features.

3.2.2. Dense large-scale feature extraction residual block

The LiDAR has a long detection range, and the features of some distant objects tend to be sparse. Although coarse-grained large-scale features are extracted using the sparse dilation convolution, the increase in the dilation rate causes a decrease in the ability to construct features for small-sized objects at long distances [44]. Therefore, fine-grained construction of long-range features is necessary for accurate 3D object detection.

To address the above problems, we propose a dense large-scale feature extraction residual block (D-LSFE-Res-Block). The block contains three branches, as shown in Fig. 3. The residual branch is utilized to prevent

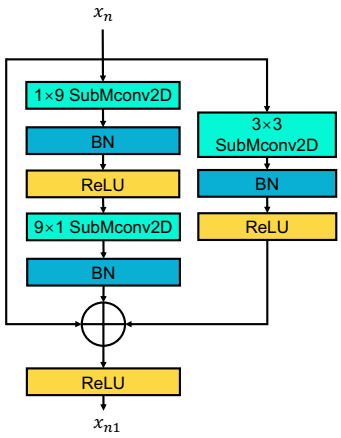

Figure 3: The dense large-scale feature extraction residual block (D-LSFE-Res-Block). D-LSFE-Res-Block consists of the residual branch, dense feature extraction branch, and dense large-scale feature extraction branch. The dense large-scale feature extraction branch consists of a 1×9 and a 9×1 submanifold sparse convolution. The dense feature extraction branch consists of a 3×3 convolution.

network performance degradation [46]. The fine-grained feature extraction branch consists of a 3×3 submanifold sparse convolution to extract fine-grained features. The dense large-scale feature extraction branch consists of a 1×9 and a 9×1 submanifold sparse convolution. The dense large-scale feature extraction branch is computationally equivalent to two 3×3 submanifold sparse convolutions, but the features constructed are farther, which constructs dense large-scale features.

3.2.3. Multi-scale feature extraction module

We propose a multi-scale feature extraction module (MSFE-Module) to extract multi-scale features of objects, as shown in Fig. 4. The module consists of an optional down-sampling block, a D-LSFE-Res-Block, and several LSFE-Res-Blocks. The down-sampling block downsamples the input using a spatially sparse convolution [15], thus retaining more complete features. All other blocks consist of submanifold sparse convolutions to avoid the feature sparsity increasing as the number of blocks increases. In Fig. 4, m denotes the dilation rate of the sparse dilation convolution in each LSFE-Res-Block. m increases gradually as the number of LSFE-Res-Blocks increases, thus gradually increasing the scale of the extracted features. The second block utilizes

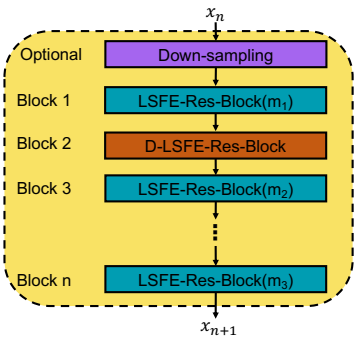

Figure 4: The proposed multi-scale feature extraction module (MSFE-Module). The module contains an optional down-sampling block, a dense large-scale feature extraction block, and several large-scale feature extraction blocks. m represents the dilated rate of the dilated sparse convolution in the block.

the D-LSFE-Res-Block, which extracts large-scale features densely and prevents the loss of objects with fewer point clouds. Hence, the multi-scale feature extraction module can simultaneously extract dense, coarse-grained large-scale, and fine-grained large-scale features.

3.3. Neck

ConvNeXt [47, 48] is often applied in object classification and detection tasks to capture multi-scale features in images. We borrowed the structure of ConvNeXt when designing the neck of PillarNeXt. The proposed neck comprises a sparse convolution module and a sparse ConvNeXt module.

Sparse ConvNeXt: As shown in Fig. 5, the proposed sparse ConvNeXt has a similar structure to ConvNeXt, but a 5×5 submanifold sparse convolution kernel [16] replaces the large-scale 7×7 convolution kernel. Due to the high sparsity of the point clouds, submanifold sparse convolution reduces ineffective convolution. In particular, we use a large-scale convolution kernel in the neck because the feature map there is smaller and does not significantly increase the computation cost.

The proposed neck is shown in Fig. 5. The neck starts with a 3×3 spatially sparse convolution module, a Batch Norm, and a ReLU activation function. Then, several sparse ConvNeXt modules extract multi-scale features from the feature map in the neck.

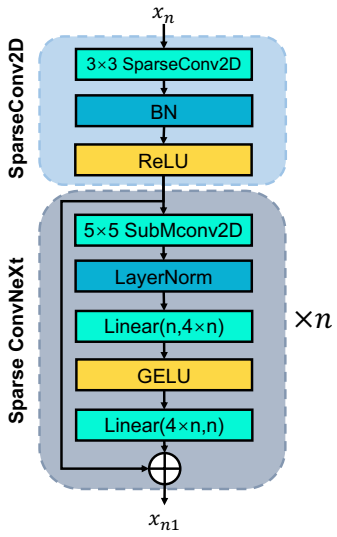

Figure 5: The neck of proposed PillarNeXt. It consists of the SparseConv2D module and the Sparse ConvNeXt module. SparseConv2D is the spatially sparse convolution. SubMconv2D is the submanifold sparse convolution.

3.4. Network

As shown in Fig. 6, the proposed PillarNeXt is similar to most 3D object detection networks, including the feature encoding, the backbone, the neck, and the detection head. The feature encoding utilizes the proposed Voxel2Pillar feature encoding. The backbone is the feature pyramid network, including six MSFE-Modules to extract multi-scale and large-scale features. We follow the VoxelNeXt [12] to fuse the feature output from the last three backbone layers to obtain multi-scale features. We used the proposed neck in the network. The detection head, also proposed by VoxelNeXt [12], directly predicts the object's class, size, and yaw from the sparse pillars.

The proposed PillarNeXt has a similar structure to VoxelNeXt-2D [12] but uses the proposed feature encoding, backbone, and neck. Therefore, the effectiveness of the proposed module can be verified by comparison with VoxelNeXt-2D.

4. Experiments

In this section, we first present the details of the implementation of the experiments. Then, the effectiveness of the proposed PillarNeXt is verified.

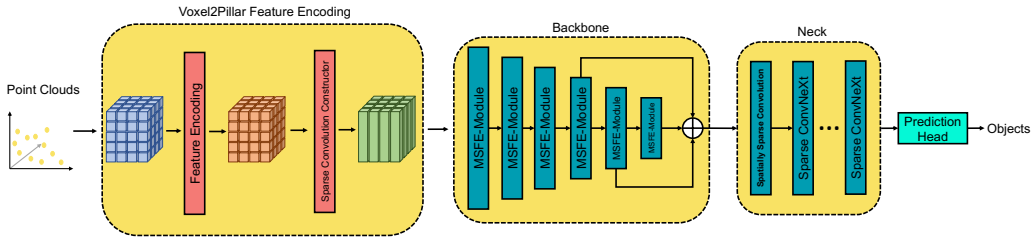

Figure 6: The proposed PillarNeXt includes a feature encode module, a backbone, a neck, and a detection head. The feature encoding module uses the proposed Voxel2Pillar feature encoding, which incorporates the advantages of both the voxel-based feature encoding and the pillar-based feature encoding. In the backbone, each layer uses the proposed multi-scale feature extraction module and combines the feature outputs of the last three layers. The proposed neck comprises a spatial sparse convolution module and several sparse ConvNeXt.

Finally, the efficacy of the proposed module is verified through ablation study.

Sec.4.1 presents the experimental setting, followed by the experimental analysis in Sec.4.2. Finally, the ablation study is presented in Sec.4.2.

4.1. Experimental setting

Datasets. Waymo Open Dataset [49] is a large-scale 3D object detection dataset in autonomous driving. The dataset is captured by high-resolution sensors (e.g., LiDAR, cameras, and radar) and contains rich annotation information (e.g., vehicles, pedestrians, and cyclists). Moreover, the dataset is rich in scenarios, including urban roads, highways, suburbs, etc., which helps train the model to be more robust. It contains 798 training sequences (160k frames) and 202 validation sequences (40k frames). It is categorized into two difficulty levels based on the number of points inside the object: LEVEL 1 means more than five points inside the object, and LEVEL 2 means at least one point but less than five points inside the object. Waymo's official evaluation metrics are the mean average precision (mAP) and the mean average precision weighted by heading (mAPH) [29]. The mAPH, which represents an increased weight on object direction prediction, is a variant of mAP.

Training and inference details. The proposed and the compared detectors utilize the official code and default profile provided by OpenPCDet[50]. All detectors are trained and tested in the same hardware environment with an A100 GPU. The training uses 20% of the training set suggested by OpenPCDet[50], and the test uses 100% of the validation set[44]. The setup of the proposed detector is consistent with the VoxelNeXt-2D [12]. In

PillarNeXt, the horizontal and vertical space detection ranges are [-75.2,75.2,-75.2,75.2] and [-2,4]; the size of the voxel is [0.1,0.1,0.2]; the size of the pillar is [0.1,0.1,6]; N in Equation 5 is set to 30.

Table 1: The performance comparison on the Waymo Open Dataset. The dataset used is Waymo, and all methods use the official code provided by OpenPCDet. All experimental data were obtained by experimenting on the same hardware environment. p and v denote the pillar-based and voxel-based detectors, respectively. Underline denotes the best-performing among all detectors. Bold indicates the best of the pillar-based detectors.

Method	Type	Vehicle (LEVEL_1)		Vehicle (LEVEL_2)		Ped. (LEVEL_1)		Ped. (LEVEL_2)		Cyc. (LEVEL_1)		Cyc. (LEVEL_2)	
		mAP	mAPH	mAP	mAPH	mAP	mAPH	mAP	mAPH	m AP	mAPH	mAP	mAPH
SECOND [15]	v	70.68	70.05	62.40	61.82	66.00	55.44	58.08	48.69	58.35	56.69	56.17	54.77
CenterPoint [29]	v	72.85	72.32	64.74	64.26	74.86	68.78	66.88	61.28	72.91	71.64	70.23	69.01
CenterPoint(resnet) [29]	v	71.05	70.49	63.01	62.50	72.29	65.87	64.27	58.41	69.90	68.65	67.32	66.12
VoxelNeXt-large [12]	v	77.50	77.01	69.04	68.59	<u>81.62</u>	<u>76.00</u>	<u>73.57</u>	<u>68.26</u>	<u>75.74</u>	<u>74.57</u>	<u>72.97</u>	<u>71.84</u>
Part-A2-Anchor [30]	v	73.41	72.86	64.73	64.23	70.46	61.35	61.32	53.23	66.97	65.56	64.50	63.14
Voxel R-CNN [11]	v	76.03	75.56	67.65	67.22	77.62	71.49	68.93	63.28	71.23	70.10	68.61	67.52
PV-RCNN [17]	v	75.16	74.54	66.58	66.01	72.42	61.20	63.42	53.42	67.00	65.31	64.52	62.90
CenterPoint(pillar) [29]	p	71.35	70.82	63.03	62.55	74.90	63.46	67.11	56.69	65.15	63.54	62.70	61.15
PointPillar [10]	p	65.91	65.24	57.81	57.21	61.93	42.60	53.63	36.85	54.26	51.07	52.22	49.14
PillarNet [31]	p	71.97	71.41	63.94	63.42	72.37	63.53	64.50	56.47	67.70	66.45	65.20	63.98
VoxelNeXt-2D [12]	p	74.40	73.89	65.93	65.48	77.40	69.10	69.10	61.49	69.57	68.31	66.96	65.75
PillarNeXt	p	<u>77.66</u>	<u>77.18</u>	<u>69.35</u>	<u>68.91</u>	**80.18**	**73.59**	**72.14**	**65.94**	**73.20**	**72.06**	**70.46**	**69.39**

4.2. Experimental analysis

The experimental results are shown in Table 1. The proposed PillarNeXt achieved the highest object detection accuracy in the vehicle detection task. Compared to voxel-based methods, the proposed PillarNeXt does not require 3D sparse convolution and has a lower computational cost but achieves higher object detection accuracy. Compared to VoxelNeXt-2D, the mAP and mAPH of LEVEL 1 have been improved by 3.26 and 3.29, respectively; the mAP and mAPH of LEVEL 2 increased by 3.42 and 3.42, respectively. Vehicle detection accuracy for both difficulty levels has been significantly improved.

In LEVEL 1 and LEVEL 2 pedestrian detection tasks, the mAP and the mAPH of the proposed PillarNeXt are only lower than VoxelNeXt-large which is based on Voxel [12]. Compared to VoxelNeXt-2D [12], pedestrian detection accuracy for both difficulty levels has been significantly improved. The mAP and mAPH of LEVEL 1 have been improved by 2.78 and 4.49, respectively; The mAP and mAPH of LEVEL 2 increased by 3.04 and 4.45, respectively. The proposed PillarNeXt improves mAPH more than mAP compared to VoxelNeXt-2D. The mAPH increases the weight of object direction detection. Therefore, the proposed PillarNeXt improves the accuracy of pedestrian direction detection more significantly.

Table 2: The ablation study of the proposed modules. Baseline is the VoxelNeXt-2D. *Multi*, *Dnese*, *Feature*, *V2P*, and *NeXt* are the LSFE-Res-Block, the D-LSFE-Res-Block, the proposed feature encoding block, the Voxel2Pillar block, and the proposed neck, respectively. The baseline is the VoxelNeXt-2D. ✓ indicates usage. In V2P, the parameter represents the size of the voxel height. In NeXt, the parameter represents the number of sparse ConvNeXt. ↑ and ↓ indicate performance improvement and degradation compared to the baseline.

Programme	Module					Vehicle (LEVEL 1)		Vehicle (LEVEL 2)		Ped. (LEVEL 1)		Ped. (LEVEL 2)		Cyc. (LEVEL 1)		Cyc. (LEVEL 2)	
	Multi	Dense	Feature	V2P	NeXt	mAP	mAPH	mAP	mAPH	mAP	mAPH	mAP	mAPH	mAP	mAPH	mAP	mAPH
Baseline						74.40	73.89	65.93	65.48	77.40	69.10	69.10	61.49	69.57	68.31	66.96	65.75
A	✓					74.96	74.44	66.57	66.10	77.22	69.21	69.14	61.72	70.20	68.92	67.55	66.32
						↑0.56	↑0.55	↑0.64	↑0.62	↓0.18	↑0.11	↑0.04	↑0.23	↑0.63	↑0.61	↑0.59	↑0.57
B	✓	✓				75.34	74.81	66.93	66.45	77.93	69.95	69.86	62.45	70.62	69.34	67.98	66.75
						↑0.96	↑0.92	↑1.00	↑0.97	↑0.53	↑0.85	↑0.76	↑0.96	↑1.05	↑1.03	↑1.02	↑1.00
C	✓	✓	✓			75.93	75.43	67.58	67.12	78.40	70.68	70.40	63.20	71.48	70.21	68.78	67.55
						↑1.53	↑1.54	↑1.65	↑1.64	↑1.00	↑1.58	↑1.30	↑1.71	↑1.91	↑1.90	↑1.82	↑1.80
D	✓	✓	✓	0.3		76.63	76.14	68.24	67.79	79.06	71.91	71.00	64.31	71.05	69.88	68.39	67.26
						↑2.23	↑2.25	↑2.31	↑2.31	↑1.66	↑2.81	↑1.90	↑2.82	↑1.43	↑1.57	↑1.43	↑1.51
E	✓	✓	✓	0.2		76.87	76.38	68.48	68.03	79.28	72.22	71.27	64.65	71.46	70.25	68.77	67.61
						↑2.47	↑2.49	↑2.55	↑2.55	↑1.88	↑3.12	↑2.17	↑3.16	↑1.87	↑1.94	↑1.81	↑1.86
F	✓	✓	✓	0.2	3	77.65	77.16	69.36	68.91	79.66	72.91	71.72	65.36	72.63	71.43	69.88	68.73
						↑3.25	↑3.27	↑3.43	↑3.43	↑2.26	↑3.81	↑2.62	↑3.87	↑3.06	↑3.12	↑2.92	↑2.98
G	✓	✓	✓	0.2	1	77.62	77.15	69.34	68.90	79.90	73.42	71.93	65.81	72.99	71.88	70.26	69.20
						↑3.22	↑3.26	↑3.41	↑3.42	↑2.50	↑4.32	↑2.83	↑4.32	↑3.42	↑3.57	↑3.30	↑3.45

In cyclist detection tasks, the detection accuracy of the PillarNeXt is only lower than the VoxelNeXt-large [12]. However, the proposed PillarNeXt outperforms all the pillar-based detectors. In addition, compared to VoxelNeXt-2D, the accuracy of cyclist detection for both difficulty levels has been significantly improved. The mAP and mAPH of LEVEL 1 have been improved by 3.63 and 3.75, respectively; The mAP and mAPH of LEVEL 2 increased by 3.50 and 3.64, respectively.

From the above analysis, the proposed PillarNeXt achieved the highest object detection accuracy in the vehicle detection task. The proposed PillarNeXt's pedestrian and cyclist detection accuracy is slightly lower than VoxelNeXt-large but higher than all the pillar-based detectors. However, the computational cost of the pillar-based detectors is much lower than that of the voxel-based detectors. Therefore, the proposed PillarNeXt can achieve more competitive detection accuracy with limited computing power.

4.3. Ablation study

Table 2 and Fig. 7 show the results of the ablation study on the proposed modules. We separately verified the effectiveness of the proposed feature encoding, backbone, and neck.

Table 3: The ablation study of the proposed neck. Size represents the size of the submanifold sparse convolution kernel in the ConvNeXt module. The baseline is VoxelNeXt-2D [12]. ↑ and ↓ indicate performance improvement and degradation compared to the baseline.

Programme	Size	Vehicle (LEVEL 1)		Vehicle (LEVEL 2)		Ped. (LEVEL 1)		Ped. (LEVEL 2)		Cyc. (LEVEL 1)		Cyc. (LEVEL 2)	
		mAP	mAPH	mAP	mAPH	mAP	mAPH	mAP	mAPH	mAP	mAPH	mAP	mAPH
Baseline		74.40	73.89	65.93	65.48	77.40	69.10	69.10	61.49	69.57	68.31	66.96	65.75
A	7	77.62	77.15	69.34	68.90	79.90	73.42	71.93	65.81	72.99	71.88	70.26	69.20
		↑3.22	↑3.26	↑3.41	↑3.42	↑2.50	↑4.32	↑2.83	↑4.32	↑3.42	↑3.57	↑3.30	↑3.45
B	5	77.66	77.18	69.35	68.91	80.18	73.59	72.14	65.94	73.20	72.06	70.46	69.39
		↑3.26	↑3.29	↑3.42	↑3.43	↑2.78	↑4.49	↑3.04	↑4.45	↑3.63	↑3.75	↑3.50	↑3.64
C	3	77.41	76.92	69.10	68.65	79.93	73.30	71.95	65.70	72.67	71.53	69.97	68.88
		↑3.01	↑3.03	↑3.17	↑3.17	↑2.53	↑4.20	↑2.85	↑4.21	↑3.10	↑3.22	↑3.01	↑3.13

4.3.1. Feature encode

In Table 2, compared to Programme B, Programme C uses the proposed voxel feature encoding module, as shown in Equation 3. Compared to Programme B, the average detection accuracy of vehicles, pedestrians, and cyclists has been improved by 0.63, 0.62, and 0.83, respectively. The proposed voxel feature encoding method shows a more significant improvement in cyclists' detection accuracy. It shows that the proposed voxel feature encoding constructs richer features, which is conducive to obtaining higher object detection accuracy.

Compared to Programme B, Programme D and E use the proposed voxel feature encoding module and Voxel2Paillar module. Programme D and E voxel sizes are [0.1, 0.1, 0.3] and [0.1, 0.1, 0.2], respectively. In Programme D, the average detection accuracy of vehicles, pedestrians, and cyclists has been improved by 1.31, 1.52, and 0.46, respectively. In Programme E, the average detection accuracy of vehicles, pedestrians, and cyclists has been improved by 1.55, 1.81, and 0.85, respectively. The experiment shows that the object detection accuracy is further improved as the voxel size decreases.

4.3.2. Backbone

In Table 2, Programme A indicates that the MSFE-Module utilized in the backbone contains only LSFE-Res-Block. In the LEVEL 1 and LEVEL 2 vehicle detection tasks, the mAP and mAPH achieved boosts between 0.55 and 0.64. The mAP and mAPH boosted between 0.57 and 0.63 in the cyclist object detection task. However, in the pedestrian object detection task, mAP decreased by 0.18 in LEVEL 1, while other metrics only showed

the highest improvement of 0.23. The above analysis shows that multi-scale features are constructed using dilated sparse convolutional branches with different dilation rates in each backbone layer, which improves the detection of large-scale objects. The coarse-grained multi-scale features constructed by dilated convolution degrade the detection performance of simple small-size pedestrians. However, the module is beneficial for detecting difficult pedestrians.

Programme B represents the addition of LSFE-Res-Block and D-LSFE-Res-Block to the MSFE-Module. Compared to Programme A, all metrics are further improved. In vehicle and cyclist detection tasks, an improvement of about 1 is achieved compared to VoxelNeXt-2D [12]. In addition, the drop in the mAP for pedestrian detection in LEVEL 1 is compensated, with an improvement of 0.53. Other pedestrian detection metrics are further improved. It shows that the multi-scale feature extraction in the backbone should combine coarse-grained large-scale feature extraction and fine-grained large-scale feature extraction. The simultaneous construction of coarse-grained large-scale and fine-grained large-scale features helps construct long-range features for large objects such as vehicles. It prevents the degradation of detection performance for small-sized objects due to large feature granularity.

4.3.3. Neck

Compared to Programme E, Programme F and G use the proposed neck. The number of sparse ConvNeXt modules used in Programme F and G is 3 and 1, respectively. There is no significant difference in the detection performance of Programme F and G in the vehicle detection task. However, compared to Programme F, Programme G improves pedestrian and cyclist detection accuracy by an average of 0.35 and 0.42, respectively. It indicates that a small number of sparse ConvNeXt modules can improve object detection accuracy. However, as the number of modules increases, the detection accuracy of small objects will decrease slightly. The excessive use of large-scale convolution kernels in the neck would reduce the ability to construct features for small objects.

Programme G improves vehicle, pedestrian, and cyclist detection accuracy by an average of 0.81, 0.91, and 1.56 compared to Programme E. Especially in the cyclist detection task, the detection accuracy has been improved by 1.53, 1.73, 1.49, and 1.59, respectively, demonstrating that the proposed neck can effectively improve the detection accuracy of cyclists. In the pedestrian detection task, mAPH improved more than mAP, indicating that the

proposed neck can significantly improve the detection ability of pedestrian direction.

Table 3 shows the ablation study on the size of sparse convolution kernels in sparse ConvNeXt. As shown in Programme B, the highest detection accuracy improvement is achieved when the kernel size of sparse convolution is 5. When the kernel size of sparse convolution is 7, the detection accuracy of small objects such as cyclists and pedestrians significantly decreases due to the constructed feature distance being too far. When the kernel size of sparse convolution is 3, compared to Programme C, the accuracy of all object detection is significantly reduced. This is because small convolution kernels cannot fully construct the long-range features of the object.

5. Conclusion

Different objects' sizes vary greatly, so extracting multi-scale and large-scale features is essential for accurate 3D object detection. We propose the PillarNeXt based on Pillar, which achieves competitive object detection accuracy while ensuring the real-time performance of 3D detectors. We have redesigned the feature encoding module, the backbone, and the neck. Our proposed Voxel2Pillar feature encoding module constructs pillars that contain richer features. The proposed fully sparse backbone network can extract multi-scale features at each layer without increasing the kernel size of convolution. We used the proposed sparse ConvNeXt in the neck. The proposed neck effectively improves the accuracy of object detection, especially for the detection of cyclists. We validate the proposed PillarNeXt and modules on the Waymo Open Dataset. The results show that the accuracy of 3D object detection has been significantly improved.

Acknowledgments

This work is supported by the Chongqing Natural Science Foundation Innovation and Development Joint Fund (CSTB2023NSCQ-LZX0109), the Chongqing Technology and Innovation Application Development Key Project (cstb2022tiad-kpx0148), and the Fundamental Research Funds for the Central Universities, China (No. 2022CDJYGRH-001).

References

[1] J. Mao, Y. Xue, M. Niu, H. Bai, J. Feng, X. Liang, H. Xu, C. Xu, Voxel transformer for 3d object detection, in: Proceedings of the IEEE/CVF International Conference on Computer Vision (ICCV), 2021, pp. 3164–3173.

[2] H. Wu, C. Wen, S. Shi, X. Li, C. Wang, Virtual sparse convolution for multimodal 3d object detection, in: Proceedings of the IEEE/CVF Conference on Computer Vision and Pattern Recognition (CVPR), 2023, pp. 21653–21662.

[3] J. Mao, M. Niu, H. Bai, X. Liang, H. Xu, C. Xu, Pyramid r-cnn: Towards better performance and adaptability for 3d object detection, in: Proceedings of the IEEE/CVF International Conference on Computer Vision (ICCV), 2021, pp. 2723–2732.

[4] H. Sheng, S. Cai, Y. Liu, B. Deng, J. Huang, X.-S. Hua, M.-J. Zhao, Improving 3d object detection with channel-wise transformer, in: Proceedings of the IEEE/CVF International Conference on Computer Vision (ICCV), 2021, pp. 2743–2752.

[5] Z. Yang, Y. Sun, S. Liu, J. Jia, 3dssd: Point-based 3d single stage object detector, in: Proceedings of the IEEE/CVF Conference on Computer Vision and Pattern Recognition (CVPR), 2020, pp. 11040–11048.

[6] X. Li, C. Wang, Z. Zeng, Ws-ssd: Achieving faster 3d object detection for autonomous driving via weighted point cloud sampling, Expert Systems with Applications 249 (2024) 123805.

[7] X. Li, A. Ren, Y. Tan, X. Li, Z. Huang, C. Wang, X. Chen, D. Liu, Vea: An fpga-based voxel encoding accelerator for 3d object detection with lidar, in: 2022 IEEE 40th International Conference on Computer Design (ICCD), IEEE, 2022, pp. 509–516.

[8] Z. Liu, H. Tang, S. Zhao, K. Shao, S. Han, Pvnas: 3d neural architecture search with point-voxel convolution, IEEE Transactions on Pattern Analysis and Machine Intelligence 44 (11) (2021) 8552–8568.

[9] X. Bai, Z. Hu, X. Zhu, Q. Huang, Y. Chen, H. Fu, C.-L. Tai, Transfusion: Robust lidar-camera fusion for 3d object detection with transformers,

in: Proceedings of the IEEE/CVF Conference on Computer Vision and Pattern Recognition (CVPR), 2022, pp. 1090–1099.

[10] A. H. Lang, S. Vora, H. Caesar, L. Zhou, J. Yang, O. Beijbom, Pointpillars: Fast encoders for object detection from point clouds, in: Proceedings of the IEEE/CVF Conference on Computer Vision and Pattern Recognition (CVPR), 2019, pp. 12697–12705.

[11] J. Deng, S. Shi, P. Li, W. Zhou, Y. Zhang, H. Li, Voxel r-cnn: Towards high performance voxel-based 3d object detection, Proceedings of the AAAI Conference on Artificial Intelligence (AAAI) 35 (2) (2021) 1201–1209.

[12] Y. Chen, J. Liu, X. Zhang, X. Qi, J. Jia, Voxelnext: Fully sparse voxelnet for 3d object detection and tracking, in: Proceedings of the IEEE/CVF Conference on Computer Vision and Pattern Recognition (CVPR), 2023, pp. 21674–21683.

[13] Y. Zhou, O. Tuzel, Voxelnet: End-to-end learning for point cloud based 3d object detection, in: Proceedings of the IEEE/CVF Conference on Computer Vision and Pattern Recognition (CVPR), 2018, pp. 4490–4499.

[14] J. Li, C. Luo, X. Yang, Pillarnext: Rethinking network designs for 3d object detection in lidar point clouds, in: Proceedings of the IEEE/CVF Conference on Computer Vision and Pattern Recognition (CVPR), 2023, pp. 17567–17576.

[15] Y. Yan, Y. Mao, B. Li, Second: Sparsely embedded convolutional detection, Sensors 18 (10) (2018) 3337.

[16] B. Graham, M. Engelcke, L. van der Maaten, 3d semantic segmentation with submanifold sparse convolutional networks, in: Proceedings of the IEEE Conference on Computer Vision and Pattern Recognition (CVPR), 2018, pp. 9224–9232.

[17] S. Shi, C. Guo, L. Jiang, Z. Wang, J. Shi, X. Wang, H. Li, Pv-rcnn: Point-voxel feature set abstraction for 3d object detection, in: Proceedings of the IEEE/CVF Conference on Computer Vision and Pattern Recognition (CVPR), 2020, pp. 10529–10538.

[18] M. Ye, S. Xu, T. Cao, Hvnet: Hybrid voxel network for lidar based 3d object detection, in: Proceedings of the IEEE/CVF Conference on Computer Vision and Pattern Recognition (CVPR), 2020, pp. 1631–1640.

[19] J. Noh, S. Lee, B. Ham, Hvpr: Hybrid voxel-point representation for single-stage 3d object detection, in: Proceedings of the IEEE/CVF Conference on Computer Vision and Pattern Recognition (CVPR), 2021, pp. 14605–14614.

[20] Y. Huang, S. Zhou, J. Zhang, J. Dong, N. Zheng, Voxel or pillar: Exploring efficient point cloud representation for 3d object detection, in: Proceedings of the AAAI Conference on Artificial Intelligence (AAAI), Vol. 38, 2024, pp. 2426–2435.

[21] A. Geiger, P. Lenz, C. Stiller, R. Urtasun, Vision meets robotics: The kitti dataset, The International Journal of Robotics Research 32 (11) (2013) 1231–1237.

[22] H. Caesar, V. Bankiti, A. H. Lang, S. Vora, V. E. Liong, Q. Xu, A. Krishnan, Y. Pan, G. Baldan, O. Beijbom, nuscenes: A multimodal dataset for autonomous driving, in: Proceedings of the IEEE/CVF Conference on Computer Vision and Pattern Recognition (CVPR), 2020, pp. 11621–11631.

[23] Y. Chen, J. Liu, X. Zhang, X. Qi, J. Jia, Largekernel3d: Scaling up kernels in 3d sparse cnns, in: Proceedings of the IEEE/CVF Conference on Computer Vision and Pattern Recognition (CVPR), 2023, pp. 13488–13498.

[24] J. Park, C. Kim, S. Kim, K. Jo, Pcscnet: Fast 3d semantic segmentation of lidar point cloud for autonomous car using point convolution and sparse convolution network, Expert Systems with Applications 212 (2023) 118815.

[25] Y. Li, Q. Hou, Z. Zheng, M.-M. Cheng, J. Yang, X. Li, Large selective kernel network for remote sensing object detection, in: Proceedings of the IEEE/CVF International Conference on Computer Vision (ICCV), 2023, pp. 16794–16805.

[26] Ding, Xiaohan and Zhang, Xiangyu and Han, Jungong and Ding, Guiguang, Scaling up your kernels to 31x31: Revisiting large kernel design in cnns, in: Proceedings of the IEEE/CVF Conference on Computer Vision and Pattern Recognition (CVPR), 2022, pp. 11963–11975.

[27] X. Ding, X. Zhang, J. Han, G. Ding, Scaling up your kernels to 31x31: Revisiting large kernel design in cnns, in: Proceedings of the IEEE/CVF Conference on Computer Vision and Pattern Recognition (CVPR), 2022, pp. 11963–11975.

[28] M. Tan, R. Pang, Q. V. Le, Efficientdet: Scalable and efficient object detection, in: Proceedings of the IEEE/CVF Conference on Computer Vision and Pattern Recognition (CVPR), 2020, pp. 10781–10790.

[29] T. Yin, X. Zhou, P. Krahenbuhl, Center-based 3d object detection and tracking, in: Proceedings of the IEEE/CVF Conference on Computer Vision and Pattern Recognition (CVPR), 2021, pp. 11784–11793.

[30] S. Shi, Z. Wang, J. Shi, X. Wang, H. Li, From points to parts: 3d object detection from point cloud with part-aware and part-aggregation network, IEEE Transactions on Pattern Analysis and Machine Intelligence 43 (8) (2021) 2647–2664.

[31] G. Shi, R. Li, C. Ma, Pillarnet: Real-time and high-performance pillar-based 3d object detection, in: European Conference on Computer Vision (ECCV), 2022, pp. 35–52.

[32] Y. Li, Y. Chen, X. Qi, Z. Li, J. Sun, J. Jia, Unifying voxel-based representation with transformer for 3d object detection, Advances in Neural Information Processing Systems (NeurIPS) 35 (2022) 18442–18455.

[33] Y. Chen, Y. Li, X. Zhang, J. Sun, J. Jia, Focal sparse convolutional networks for 3d object detection, in: Proceedings of the IEEE/CVF Conference on Computer Vision and Pattern Recognition (CVPR), 2022, pp. 5428–5437.

[34] X. Xu, Z. Wang, J. Zhou, J. Lu, Binarizing sparse convolutional networks for efficient point cloud analysis, in: Proceedings of the IEEE/CVF Conference on Computer Vision and Pattern Recognition (CVPR), 2023, pp. 5313–5322.

[35] T.-Y. Lin, P. Dollar, R. Girshick, K. He, B. Hariharan, S. Belongie, Feature pyramid networks for object detection, in: Proceedings of the IEEE Conference on Computer Vision and Pattern Recognition (CVPR), 2017, pp. 2117–2125.

[36] K. Min, G.-H. Lee, S.-W. Lee, Attentional feature pyramid network for small object detection, Neural Networks 155 (2022) 439–450.

[37] Y. Quan, D. Zhang, L. Zhang, J. Tang, Centralized feature pyramid for object detection, IEEE Transactions on Image Processing 32 (2023) 4341–4354.

[38] Z. Huang, H. Dai, T.-Z. Xiang, S. Wang, H.-X. Chen, J. Qin, H. Xiong, Feature shrinkage pyramid for camouflaged object detection with transformers, in: Proceedings of the IEEE/CVF Conference on Computer Vision and Pattern Recognition (CVPR), 2023, pp. 5557–5566.

[39] L.-C. Chen, G. Papandreou, I. Kokkinos, K. Murphy, A. L. Yuille, Deeplab: Semantic image segmentation with deep convolutional nets, atrous convolution, and fully connected crfs, IEEE Transactions on Pattern Analysis and Machine Intelligence 40 (4) (2017) 834–848.

[40] P. Mittal, A. Sharma, R. Singh, V. Dhull, Dilated convolution based rcnn using feature fusion for low-altitude aerial objects, Expert Systems with Applications 199 (2022) 117106.

[41] Y. Li, Y. Chen, N. Wang, Z. Zhang, Scale-aware trident networks for object detection, in: Proceedings of the IEEE/CVF International Conference on Computer Vision (ICCV), 2019, pp. 6054–6063.

[42] W. Mao, T. Wang, D. Zhang, J. Yan, O. Yoshie, Pillarnest: Embracing backbone scaling and pretraining for pillar-based 3d object detection, IEEE Transactions on Intelligent Vehicles (2024) 1–10.

[43] Z. Cao, T. Wang, P. Sun, F. Cao, S. Shao, S. Wang, Scorepillar: A real-time small object detection method based on pillar scoring of lidar measurement, IEEE Transactions on Instrumentation and Measurement 73 (2024) 1–13.

[44] J. Liu, Y. Chen, X. Ye, Z. Tian, X. Tan, X. Qi, Spatial pruned sparse convolution for efficient 3d object detection, Advances in Neural Information Processing Systems (NeurIPS) 35 (2022) 6735–6748.

[45] Q. Chen, Y. Wang, T. Yang, X. Zhang, J. Cheng, J. Sun, You only look one-level feature, in: Proceedings of the IEEE/CVF Conference on Computer Vision and Pattern Recognition (CVPR), 2021, pp. 13039–13048.

[46] K. He, X. Zhang, S. Ren, J. Sun, Deep residual learning for image recognition, in: Proceedings of the IEEE/CVF Conference on Computer Vision and Pattern Recognition (CVPR), 2016, pp. 770–778.

[47] Z. Liu, H. Mao, C.-Y. Wu, C. Feichtenhofer, T. Darrell, S. Xie, A convnet for the 2020s, in: Proceedings of the IEEE/CVF Conference on Computer Vision and Pattern Recognition (CVPR), 2022, pp. 11976–11986.

[48] S. Woo, S. Debnath, R. Hu, X. Chen, Z. Liu, I. S. Kweon, S. Xie, Convnext v2: Co-designing and scaling convnets with masked autoencoders, in: Proceedings of the IEEE/CVF Conference on Computer Vision and Pattern Recognition (CVPR), 2023, pp. 16133–16142.

[49] P. Sun, H. Kretzschmar, X. Dotiwalla, A. Chouard, V. Patnaik, P. Tsui, J. Guo, Y. Zhou, Y. Chai, B. Caine, et al., Scalability in perception for autonomous driving: Waymo open dataset, in: Proceedings of the IEEE/CVF Conference on Computer Vision and Pattern Recognition (CVPR), 2020, pp. 2446–2454.

[50] O. D. Team, Openpcdet: An open-source toolbox for 3d object detection from point clouds, `https://github.com/open-mmlab/OpenPCDet` (2020).

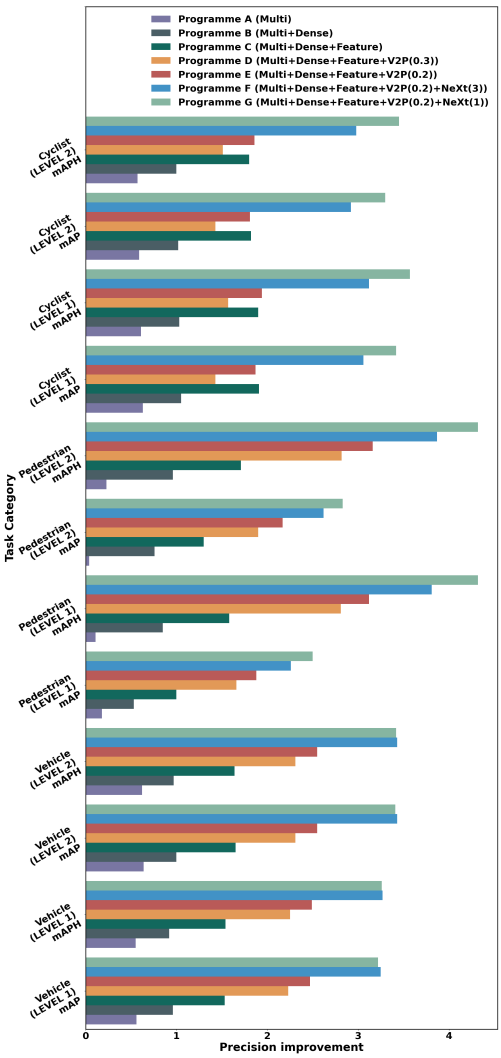

Figure 7: Comparison of precision improvement after using different modules compared to the baseline.